Experimental Evaluation of the Inertia Properties of Large Diesel Engines

Mohammad Afzal[(1)], Kari Saine[(2)], Claus Paro[(2)], and Eddy Dascotte[(3)]

[1] KTH Royal Institute of Technology
The Marcus Wallenberg Laboratory for Sound and Vibration Research (MWL)
SE 100 44 Stockholm, Sweden

[2] Wärtsilä Finland Oy
Research and Development, WSSC
P.O. Box 321, 65101 Vaasa, Finland

[3] Dynamic Design Solutions (DDS) NV
Interleuvenlaan 64-3001 Leuven, Belgium

ABSTRACT
Inertia properties of several medium speed large diesel engines are evaluated using the Inertia Restrain Method (IRM). This method requires measuring frequency response functions (FRFs) at several well-chosen locations and under dynamic loading in different directions that stimulate rigid body movements. The mass line values of the measured FRFs are then evaluated and, together with the sensor locations, are used by IRM to determine center of gravity, mass and mass moments of inertia.

The aim of the study is to investigate the accuracy and robustness of the IRM for extracting the inertia properties of complex structures. Therefore, several line- and V-engines were measured. The experimental results are compared with finite element models and result obtained from weighing tests. Different types of excitation source such as hammer and shaker are used to excite the structure. The result obtained from two excitation sources are compared and discussed. The effect of measurement point locations and driving point accelerometers on the FRFs and inertia properties are investigated.

The extracted inertia properties in all cases are considered sufficiently accurate. This indicates that the IRM is a robust tool for identifying the inertia properties of large and complex structures and can be employed at an industrial level.

Keywords: Inertia restrain method, Mass line, Diesel engine, Inertia properties, Frequency response functions.

INTRODUCTION

Accurate prediction of the rigid body modes is essential for medium speed large diesel engines to avoid a large displacement at low frequencies. Due to a variation in the dynamic stiffness of engine mounts and partially known inertia properties, this becomes a challenging task. Accurate values of the inertia properties are often unknown since an accurate finite element (FE) model of the full engine is seldom available due to the complex nature of the engine components. A weighing test is used at Wärtsilä Finland Oy to determine the mass of engines and center of gravity in the longitudinal and transversal directions. However, the moment of inertias and the center of gravity in the vertical direction cannot be determined by the weighing test.

As all ten inertia properties of a complex structure cannot be easily determined, this has led to the development of several experimental based methods in last decades [1–4]. Among the developed methods, the Inertia Restrain Method (IRM) is known to be relatively insensitive to the measurement noises [5, 6]. The IRM uses the frequency response function (FRF) mass-line values to compute the inertia properties as presented by many researchers [7, 8]. Different variants of the IRM are proposed in the literature [2, 4, 9, 10]. The method presented in Ref. [4] is implemented in the FEMtools commercial software [11] that was used in this study. The advantage of this method is that the procedure is non-iterative and inertia properties are obtained through a direct solution of two linear problems.

The objective of this study is to apply the IRM tool as implemented in the Rigid Body Property Extractor module (RBPE) of FEMtools on heavy and complex structures such as medium speed large diesel engines and investigate the robustness of the tool for the industrial application. Several line and V-engines are measured to achieve the goal. The accuracy of the IRM depends on the selection of measurement and excitation points and directions since the linear problems require several inversions. In order to minimize these errors, the recommendations outlined in Refs. [5, 11] are taken into consideration. The obtained inertia properties are compared with finite element data if available and weighing test results. The effect of the measurement and excitation points on the FRFs and inertia properties are analysed experimentally. The obtained results are discussed in detail.

THEORETICAL BACKGROUND

The IRM procedure requires the mass-line values as input, obtained from measured FRFs, see [4]. Precise values of the mass-line are required for a good estimate of the inertia properties. To compute the inertia properties, kinematics and dynamics equations are solved separately. To derive the required equations, consider the structure illustrated in Figure 1 with its origin at o and centre of gravity (COG) at point c defined by the coordinates (x_c, y_c, z_c) .

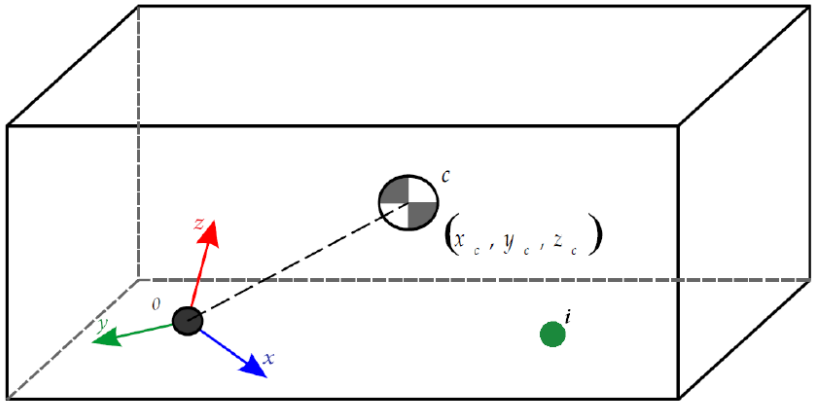

Figure 1: Center of gravity, origin and a general point i.

The kinematic relationship between the acceleration at a general point, *i* and the origin is

$$\begin{bmatrix} \ddot{x}_i \\ \ddot{y}_i \\ \ddot{z}_i \end{bmatrix} = \begin{bmatrix} \ddot{x}_o \\ \ddot{y}_o \\ \ddot{z}_o \end{bmatrix} + \begin{bmatrix} 0 & z_i & -y_i \\ -z_i & 0 & x_i \\ y_i & -x_i & 0 \end{bmatrix} \begin{bmatrix} \ddot{\theta}_x \\ \ddot{\theta}_y \\ \ddot{\theta}_z \end{bmatrix}, \tag{1}$$

where $(\ddot{x}_o, \ddot{y}_o, \ddot{z}_o, \ddot{\theta}_x, \ddot{\theta}_y, \ddot{\theta}_z)$ are the rigid body acceleration at origin and $(\ddot{x}_i, \ddot{y}_i, \ddot{z}_i)$ denotes the acceleration at a general point *i*. To obtain the angular acceleration at origin without measuring the translational acceleration at the origin, equation (1) is re-arranged as

$$\begin{bmatrix} \ddot{x}_i/F \\ \ddot{y}_i/F \\ \ddot{z}_i/F \end{bmatrix} = \underbrace{\begin{bmatrix} 1 & 0 & 0 & 0 & z_i & -y_i \\ 0 & 1 & 0 & -z_i & 0 & x_i \\ 0 & 0 & 1 & y_i & -x_i & 0 \end{bmatrix}}_{\Psi} \begin{bmatrix} \ddot{x}_o/F \\ \ddot{y}_o/F \\ \ddot{z}_o/F \\ \ddot{\theta}_x/F \\ \ddot{\theta}_y/F \\ \ddot{\theta}_z/F \end{bmatrix}, \tag{2}$$

where *F* is an applied force at any co-ordinate's directions. Now, the massline values can be directly substituted to equation (2). To solve the equation, minimum 6 response directions and one excitation direction are required, thus two sets of equation (2). However, the equation is solved in a least-squares sense using all available massline values. Moreover, the solution requires the pseudo-inverse of matrix Ψ. It means that the rank of matrix Ψ must be equal to 6. This leads to some constraints in the selection of measurement and excitation directions, such as that the acceleration measured at one point cannot be used for more than two directions (using a tri-axial accelerometer). More details are described in Refs. [5, 11].

If the structure is considered as perfectly rigid and unconstrained, then the linearized dynamic equation of motion with respect to COG is given by

$$\begin{bmatrix} m & 0 & 0 & 0 & 0 & 0 \\ 0 & m & 0 & 0 & 0 & 0 \\ 0 & 0 & m & 0 & 0 & 0 \\ 0 & 0 & 0 & J_{\mathrm{xx}} & -J_{\mathrm{xy}} & -J_{\mathrm{xz}} \\ 0 & 0 & 0 & -J_{\mathrm{yx}} & J_{\mathrm{yy}} & -J_{\mathrm{yz}} \\ 0 & 0 & 0 & -J_{\mathrm{zx}} & -J_{\mathrm{zy}} & J_{\mathrm{zz}} \end{bmatrix} \begin{bmatrix} \ddot{x}_{\mathrm{c}} \\ \ddot{y}_{\mathrm{c}} \\ \ddot{z}_{\mathrm{c}} \\ \ddot{\theta}_x \\ \ddot{\theta}_y \\ \ddot{\theta}_z \end{bmatrix} = \begin{bmatrix} f_x \\ f_y \\ f_z \\ t_x \\ t_y \\ t_z \end{bmatrix}_{\mathrm{c}}, \tag{3}$$

Where $(f_x, f_y, f_z, t_x, t_y, t_z)$ is the force vector at the COG and ten unknown inertia properties m, $x_c, y_c, z_c, J_{xx}, J_{yy}, J_{zz}$, J_{xy}, J_{yz} and J_{zx} are to be determined from equation (3). To compute the required properties, moments (t_x, t_y, t_z) and acceleration of the COG $(\ddot{x_c}, \ddot{y_c}, \ddot{z_c})$ must be eliminated from the equation, and coordinates of COG x_c, y_c, z_c be introduced. The following equations are used for this purpose.

A relation between the force and moments at COG reads as

$$\begin{bmatrix} t_x \\ t_y \\ t_z \end{bmatrix}_{\mathrm{c}} = \begin{bmatrix} 0 & z_i - z_{\mathrm{c}} & -(y_i - y_{\mathrm{c}}) \\ -(z_i - z_{\mathrm{c}}) & 0 & x_i - x_{\mathrm{c}} \\ y_i - y_{\mathrm{c}} & -(x_i - x_{\mathrm{c}}) & 0 \end{bmatrix} \begin{bmatrix} f_x \\ f_y \\ f_z \end{bmatrix}_{\mathrm{c}}, \tag{4}$$

and to eliminate the COG acceleration, the following relationship is used in addition to equation (1).

$$\begin{bmatrix} \ddot{x}_i \\ \ddot{y}_i \\ \ddot{z}_i \end{bmatrix} = \begin{bmatrix} \ddot{x}_{\mathrm{c}} \\ \ddot{y}_{\mathrm{c}} \\ \ddot{z}_{\mathrm{c}} \end{bmatrix} + \begin{bmatrix} 0 & z_i - z_{\mathrm{c}} & -(y_i - y_{\mathrm{c}}) \\ -(z_i - z_{\mathrm{c}}) & 0 & x_i - x_{\mathrm{c}} \\ y_i - y_{\mathrm{c}} & -(x_i - x_{\mathrm{c}}) & 0 \end{bmatrix} \begin{bmatrix} \ddot{\theta}_x \\ \ddot{\theta}_y \\ \ddot{\theta}_z \end{bmatrix}. \tag{5}$$

Using equations (1), (4) and (5), the linearized dynamic equation of motion (3) may be rearranged to construct the system shown below where the coefficient matrix contains the known acceleration responses obtained from equation (2). The resulting equations are

$$\begin{bmatrix} 0 & -m\ddot{\theta}_z & m\ddot{\theta}_y & 0 & 0 & 0 & 0 & 0 & 0 \\ m\ddot{\theta}_z & 0 & -m\ddot{\theta}_x & 0 & 0 & 0 & 0 & 0 & 0 \\ -m\ddot{\theta}_y & m\ddot{\theta}_x & 0 & 0 & 0 & 0 & 0 & 0 & 0 \\ 0 & F_z & -F_y & \ddot{\theta}_x & 0 & 0 & -\ddot{\theta}_y & 0 & -\ddot{\theta}_z \\ -F_z & 0 & F_x & 0 & \ddot{\theta}_y & 0 & -\ddot{\theta}_x & -\ddot{\theta}_z & 0 \\ F_y & -F_x & 0 & 0 & 0 & \ddot{\theta}_z & 0 & -\ddot{\theta}_y & -\ddot{\theta}_x \end{bmatrix} \begin{bmatrix} x_c \\ y_c \\ z_c \\ J_{xx} \\ J_{yy} \\ J_{zz} \\ J_{xy} \\ J_{yz} \\ J_{xz} \end{bmatrix} = \begin{bmatrix} F_x - m\ddot{x}_o \\ F_y - m\ddot{y}_o \\ F_z - m\ddot{z}_o \\ y_i F_z - z_i F_y \\ z_i F_x - x_i F_z \\ x_i F_y - y_i F_x \end{bmatrix}, \tag{6}$$

in which the first 3 equations are uncoupled from the others. Therefore, equation (6) is solved in two steps. Moving the mass term to the left side, the first set of the equation is written as

$$\begin{bmatrix} \ddot{x}_o & 0 & -\ddot{\theta}_z & \ddot{\theta}_y \\ \ddot{y}_o & \ddot{\theta}_z & 0 & -\ddot{\theta}_x \\ \ddot{z}_o & -\ddot{\theta}_y & \ddot{\theta}_x & 0 \end{bmatrix} \begin{bmatrix} m \\ mx_c \\ my_c \\ mz_c \end{bmatrix} = \begin{bmatrix} F_x \\ F_y \\ F_z \end{bmatrix}. \tag{7}$$

The mass and COG values are determined using equation (7). In the next step, the inertia values are computed by using the second set of equation (6) after adding the previously computed mass and COG contributions. In practice, only one load case (say F_x) is used at a time to solve equation (7) and therefore, the actual equation is

$$\begin{bmatrix} \ddot{x}_o/F_x & 0 & -\ddot{\theta}_z/F_x & \ddot{\theta}_y/F_x \\ \ddot{y}_o/F_x & \ddot{\theta}_z/F_x & 0 & -\ddot{\theta}_x/F_x \\ \ddot{z}_o/F_x & -\ddot{\theta}_y/F_x & \ddot{\theta}_x/F_x & 0 \end{bmatrix} \begin{bmatrix} m \\ mx_c \\ my_c \\ mz_c \end{bmatrix} = \begin{bmatrix} 1 \\ 0 \\ 0 \end{bmatrix}, \tag{8}$$

in which mass-line values can be directly substituted. Note that with this formulation, 3 load cases are required to identify all rigid body mass property terms. However, with 2 load cases, it is possible to identify the mass and COG terms using the first step described above. Furthermore, the above formulation can be easily adapted to the case of an imposed mass, m.

EXPERIMENTAL RESULTS

To validate the robustness of the RBPE module developed by Dynamic Design Solutions (DDS) as an add-on module to FEMtools, several Wärtsilä engines are measured. The engines are mounted on soft steel springs to minimize the effect of rigid body modes on the mass-line. Eight measurement points and four load cases are measured to collect the sufficient number of FRFs data for extracting the inertia properties. The guideline presented in Ref. [5] is considered for choosing the measurement and excitation directions. Three examples are presented in this section and obtained results are discussed in detail.

Example 1

In this example, a W16V32E engine block that weighs ~20 ton is measured and inertia properties are compared with the finite element data. W16V32E stands for Wärtsilä 16 cylinders V engine with 320 [mm] bore diameter. The engine block is chosen because an accurate FE model is available. The measurement setup and FE model of the engine block are depicted in Figure 2. Hammer excitation is given in four directions (at points 1 and 2 in the transversal and vertical directions) and four response locations (1, 2, 7 and 8) are chosen to capture the required FRFs. The initial plan was to measure only the bare engine block. However, during the actual measurement, the engine block was assembled with cylinder liners as shown in Figure 2. The cylinder liners add both mass and stiffness to the structure. Nevertheless, it does not affect the compared results as the liners are also in added to the FE model.

The obtained results are shown in Table 1. The result shows a close agreement with the calculation and deviation in the absolute values are within 5% for most of the inertia properties. In some cases, the error percentage is high, however the deviation in terms of the magnitude is within the acceptable limit. The error in the cross moment of inertia is rather high. Nevertheless, the magnitude of these inertia terms is small and therefore it will have a little effect on the calculation of rigid body modes.

In FEMtools RBPE, the mass of the structure, which is often known from a weighing test, can be enforced. The mass enforcement resulted in a better agreement between the inertia values. Therefore, it is recommended, if available from a weighing test, to use the mass of the structure in the RBPE tool. However, this does not improve the computation of COG locations.

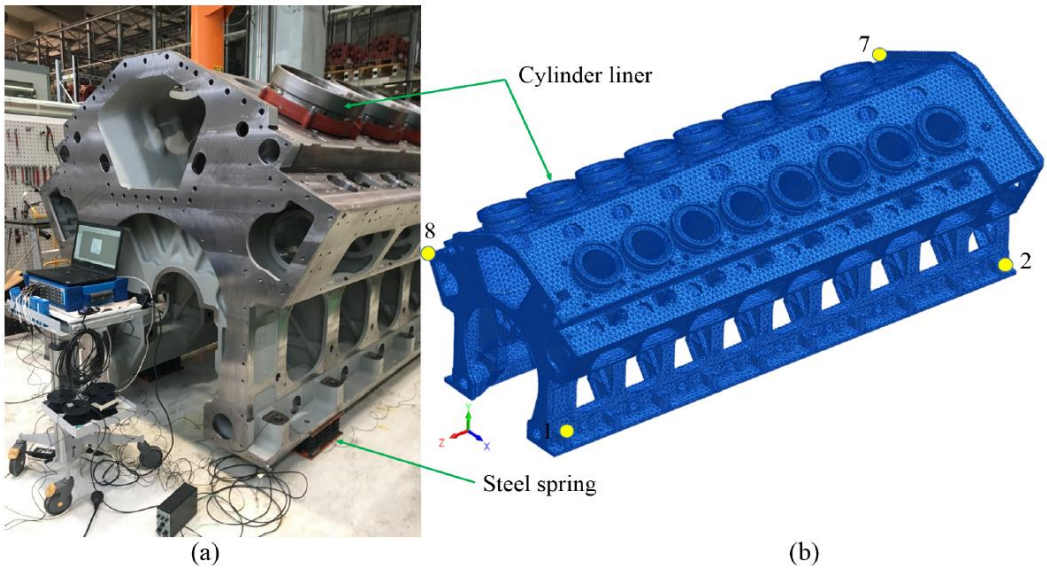

Figure 2: (a) Measurement setup and (b) finite element model of a W16V32E engine block with the cylinder liner. Measurement points are numbered 1, 2, 7 and 8 and excitations are given at points 1 and 2 in the transversal and vertical directions.

Inertia properties	FE values	Extracted values	Error	With enforced mass	Error
Mass [tn]	21.4	20.8	2.8%	21.4	0%
x_c [mm]	-0.2	-1.0	400%	-1.0	-500%
y_c [mm]	500.7	526.0	-4.9%	526.0	-4.9%
z_c [mm]	2583.6	2575.6	0.3%	2575.0	0.3%
J_{xx} [kg.m^2]	56566	53816	4.8%	57037	0.8%
J_{yy} [kg.m^2]	56733	55157	2.8%	58459	-3.0%
J_{zz} [kg.m^2]	12902	11115	13.8%	11780	8.7%
J_{xy} [kg.m^2]	-5	994	-	1053	-
J_{yz} [kg.m^2]	-453	-381	15.9%	-404	10.8%
J_{zx} [kg.m^2]	92	131	-44.5%	139	-51%

Table 1: Inertia properties of the W16V32E engine block and its comparison with finite element values.

Example 2

Frequency response functions measurement of a complete W8L20DF engine is performed in this example. A hammer (tip mass = 2.57 kg) is used to excite the structure and data is acquired using the NVGate data acquisition system.

Five excitation directions (four in the feet, one in the top corner of the engine block), and 8 corners of the engine block are chosen as the response locations. The corners are selected to avoid the local resonance of the engine components that may contaminate the FRFs data.

A complete set of FRFs are also measured after shifting a driving point and one non-driving point accelerometer (see Figure 3). The excitation locations are the same in both cases (before and after shifting the response locations). Theoretically, moving a non-driving point measurement location should not affect the computed values whereas moving a driving point accelerometer could have a significant influence on the FRF and hence on the inertia properties.

It can be difficult to measure the response and excitation at the same location and therefore it is important to study the sensitivity of the driving point FRF. It is also noticed during the measurements that in many cases the quality of driving point FRFs is not adequate.

The obtained results are compared in Table 2. They are fairly close to each other, indicating that a shift in the driving point excitation location has a marginal effect on the inertia properties. This result is important for the case where it is not possible to keep the accelerometer and excitation source very close to each other.

The deviation in the moment of inertia is larger compared to the mass value and COG. This corresponds well with the statistical error analysis presented in Ref. [5]. Note that in this case, the distance between driving point response and excitation location is 330 [mm] (15% of the total length) which is fairly large. A similar result is obtained with another engine (W8L34DF) but using a shaker excitation. This is reported in next example 3.

(a) New location of driving point

(b) New location for non-driving point

Figure 3: New locations for the driving point and non-driving points.

To further investigate the above finding, the real part of the driving point FRFs are compared in Figure 4. The real part of the FRFs is considered here because that is used to extract the inertia properties. The curves show that the mass-line for all three directions are very close although there are some discrepancies at higher frequencies. This corresponds well with the obtained results. Moreover, this also indicates the robustness of the tool. It means that even a large shift in the measurement location has a marginal effect on the inertia properties. At least, this is true for a large and heavy structure like investigated in this paper. In practice, the driving response point has a smaller shift compared to the present case.

Inertia properties	Weighing result	Extracted result	Error	Extracted using shifted points	Error
Mass [tn]	11.78	11.43	-3.1%	11.27	1.4%
x_c [mm]	1364	1367	0.2%	1387	-1.5%
y_c [mm]	82.6	89.2	7.4%	88.1	1.2%
z_c [mm]	NA	458.1	NA	458.1	NA
J_{xx} [kg.m^2]	NA	3690	NA	3485	NA
J_{yy} [kg.m^2]	NA	15093	NA	15516	NA
J_{zz} [kg.m^2]	NA	12829	NA	10019	NA
J_{xy} [kg.m^2]	NA	-738	NA	-819	NA
J_{yz} [kg.m^2]	NA	-648	NA	-92	NA
J_{zx} [kg.m^2]	NA	-1165	NA	-780	NA

Table 2: Comparison of evaluated inertia properties and weighing test results for W8L20DF engine.

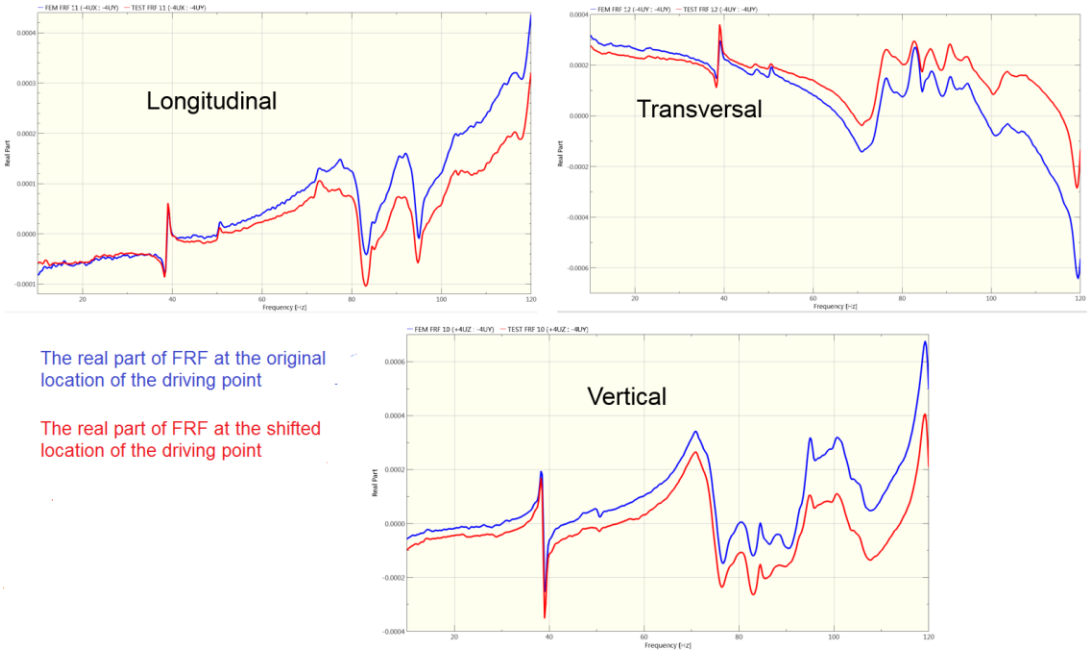

Figure 4: The effect of shifting the driving point location on the real part of the FRF [Frequency axis is 10-120 Hz].

Example 3

The frequency response functions measurement is performed on a rather heavy W8L34DF engine (~40 ton), using both hammer and shaker excitations.

Two sources of excitation are employed as it was uncertain that the hammer will be able to excite the low frequency mass-line region. The shaker excitation is applied using a hydraulic shaker as shown in Figure 5. Using a shaker, it is rather difficult to apply the excitation in the transversal and horizontal directions. Whereas, to extract all the inertia properties, all

excitations (minimum 3) must not be in the same direction. To circumvent the problem, a fixture is designed to provide the excitation at an angle of 20 degrees from the vertical direction as shown in Figure 5(b).

Five excitation directions are chosen with a hammer and four excitation directions (two in vertical and two at an angle) are employed in the shaker test. In both cases, 8 response points are measured on the corners of the engine block.

The obtained results are presented in Table 3. The mass and the COG in the x-direction are very close to the weighing results, but some deviation is seen in the transversal direction. However, the deviation in terms of the magnitude is within the acceptable limit.

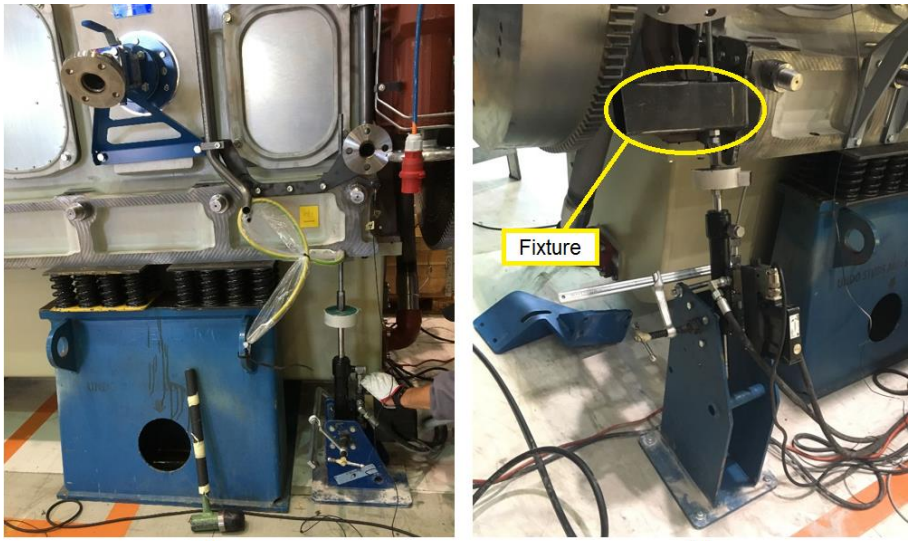

Figure 5: (a) Vertical and (b) angle excitation using the hydraulic shaker.

Inertia properties	Weighing result	Hammer excitation	Error	Shaker excitation	Error
Mass [tn]	42.76	43.61	-2.0%	41.82	2.1%
x_c [mm]	2197	2240	-1.9%	2206	-0.4%
y_c [mm]	45	31	31%	54	20%
z_c [mm]	NA	681	NA	675	NA
J_{xx} [kg.m^2]	NA	27206	NA	28930	NA
J_{yy} [kg.m^2]	NA	130079	NA	133727	NA
J_{zz} [kg.m^2]	NA	127931	NA	147819	NA
J_{xy} [kg.m^2]	NA	3716	NA	3245	NA
J_{yz} [kg.m^2]	NA	-10578	NA	-6900	NA
J_{zx} [kg.m^2]	NA	9217	NA	12888	NA

Table 3: Comparison of the evaluated inertia properties and weighing test results for W8L34DF engine.

The comparison between hammer and shaker results reveal small discrepancies that may be due to a better signal-to-noise ratio in the case of shaker excitation. However, it is hard to say that the shaker result is more accurate compared to the hammer test without good reference data.

The main conclusion of the analysis is that both the hammer and shaker excitations can be used to extract the inertia properties of a W34 line engine as the results are very close to each other. However, a shaker excitation must be used in the case of a W32 V-engine which is twice heavier than the line engines. On the other hand, hammer excitation is sufficient in the case of a W20 engine and it is much faster compared to a shaker excitation measurement setup.

A complete set of FRFs is also measured after shifting a driving point location in the vertical excitation. The extracted inertia properties are exactly the same in this case that indicates that the small shift in the driving point measurement location has no or marginal (see, example 2) effect on the inertia properties. Note that the excitation point is the same in both cases. The real part of the driving point FRFs shows that the mass line for all three directions are very close eventhough there are some discrepancies at higher frequencies. This corresponds well with the obtained results.

REMARKS AND PRACTICAL SUGGESTIONS ON THE MEASUREMENT PROCEDURES

The IRM uses the measured FRFs to extract the inertia properties implying that FRFs with high signal-to-noise ratio will lead to an accurate result. Nevertheless, based on our experience with testing the diesel engines, a few additional guidelines must be considered while performing these measurements as stated below:

- The coordinates of the excitation and response locations should be marked as accurate as possible.
- Minimum three excitation directions are required to extract the inertia properties. However, it is recommended to use 4-5 excitation directions if possible. Furthermore, the excitation location must be stiff and flat.
- Only a few response directions (6-8) are required, however the same response locations must be measured for each excitation direction.
- Only one coordinate system can be used at one point (local or global). It means that if an excitation is given in the vertical direction at one point then another excitation cannot not be at an angle at the same point. A workaround is to duplicate the point with different coordinate system.
- It is essential to measure driving point FRFs for each excitation direction in the same coordinate system.
- Rigid body natural frequencies are not of interest for these measurements. However, they should be kept as low as possible such that the lowest elastic mode is at least twice of the highest rigid body mode.
- The structure should be mounted on flexible springs. Hanging the engine with soft connections has not yielded a satisfactory result to the authors.

CONCLUSION

In this study, the rigid body inertia properties of several Wärtsilä engines are extracted using the inertia restrain method, available as an add-on specialist tool (RBPE) in the FEMtools software. Experimental results are compared with finite element data and weighing test results.

The obtained results reveal that the evaluated rigid body inertia properties are in close agreement with the weighing test and finite element results. The deviation of the values is within 5%. This is a promising result and indicates that the IRM can be potentially used for the identification of rigid body inertia properties for massive diesel engines. The inertia properties obtained using two different excitation sources (hammer and shaker) are also in good agreement. The selection of the excitation source mainly depends on the weight of the structure.

The effect of shifting the driving and non-driving point accelerometer locations is also investigated. The results show that the IRM predicts the inertia properties quite well and has a marginal effect of shifting (5- 8% of the maximum length) the driving point accelerometer and sometimes it has no effect on the properties. This shows that the IRM is a robust tool for identifying the inertia properties of large and heavy structures.

ACKNOWLEDGEMENTS
This research is funded by Wärtsilä Finland Oy.

REFERENCES

[1] M. A. Lamontia, On the determination and use of residual fexibilities, inertia restraints and rigid body modes, in: Proceedings of the 1st IMAC, Orlando, FL, 1982.
[2] J. Bretl, P. Conti, Rigid body mass properties from test data, in: Proceedings of the 5th IMAC, London, 1987.
[3] O. Nuutila, K. Saine, J. Toivola, Experimental methods for determining rigid body inertia properties from frequency response function of medium speed diesel engines, in: Proceedings of the 11th International Modal Analysis Conference, 1993, pp. 1121–1125.
[4] A. Fregolent, A. Sestieri, Identification of rigid body inertia properties from experimental data, Mechanical Systems and Signal Processing 10 (6) (1996) 697–709.
[5] H. LEE, Y. B. LEE, Y. S. PARK, Response and excitation points selection for accurate rigid-body inertia properties identification, Mechanical Systems and Signal Processing 13 (1999) 571–592.
[6] J. Toivola, O. Nuutila, Comparison of three methods for determining rigid body inertia properties from frequency response functions, in: Proceedings of the 11th International Modal Analysis Conference, 1993, pp. 1126–1132.
[7] M. Furusawa, T. Tominaga, Rigid body modes enhancement and rdof estimation for experimental modal analysis, in: Proceedings of the 4th IMAC, Los Angeles, CA, 1986.
[8] J. Crowley, T. Rockrin, D. Brown, Use of rigid body calculations in tests, in: Proceedings of the 4th IMAC, Los Angeles, CA, 1986.
[9] Y. S. Wei, J. Reis, Experimental determination of rigid body inertia properties, in: Proceedings of 6th IMAC, Las Vegas, NV, 1989.
[10] M. Furusawa, A method of determining rigid body inertia properties, in: Proceedings of the 6th IMAC, Las Vegas, NV, 1989.
[11] FEMtools Rigid Body Properties Extractor (RBPE) User Guide (2019), https://www.femtools.com.